Title
The importance of earthquake interactions for injection-induced seismicity: Retrospective modeling of the Basel Enhanced Geothermal System

Journal
Geophysical Research Letters, 43(10)

ISSN
0094-8276

Authors
Catalli, Flaminia
Rinaldi, Antonio P
Gischig, Valentin
et al.

Publication Date
2016-05-28

DOI
10.1002/2016gl068932

Peer reviewed

The importance of earthquake interactions for injection-induced seismicity: Retrospective modeling of the Basel Enhanced Geothermal System

Flaminia Catalli[1,2], Antonio P. Rinaldi[2], Valentin Gischig[3], Massimo Nespoli[4], and Stefan Wiemer[2]

[1] GeoForschungsZentrum Potsdam, Telegrafenberg, Potsdam, Germany, [2] Swiss Seismological Service, Swiss Federal Institute of Technology, ETHZ, Zürich, Switzerland, [3] Swiss Competence Center for Energy Research Supply of Electricity), Swiss Federal Institute of Technology, ETHZ, Zürich, Switzerland, [4] Istituto Nazionale di Geofisica e Vulcanologia, Bologna, Italy

Correspondence to: F. Catalli, fcatalli@gfz-potsdam.de

Abstract

We explore the role of earthquake interactions during an injection-induced seismic sequence. We propose a model, which considers both a transient pressure and static stress redistribution due to event interactions as triggering mechanisms. By calibrating the model against observations at the Enhanced Geothermal System of Basel, Switzerland, we are able to reproduce the time behavior of the seismicity rate. We observe that considering earthquake interactions in the modeling leads to a larger number of expected seismic events (24% more) if compared to a pressure-induced seismicity only. The increase of the number of events is particularly evident after the end of the injection. We conclude that implementing a model for estimating the static stress changes due to mutual event interactions increases significantly the understanding of the process and the behavior of induced seismicity.

1 Introduction

Enhanced Geothermal Systems (EGS) have recently drawn the attention of the seismological community because of the seismicity induced by reservoir stimulation. Cases of induced seismicity have been documented in a number of EGS projects [*Evans et al*., 2012; *Zang et al*., 2014]. A major challenge in EGS projects is the modeling of induced seismicity and the understanding of conditions leading to hazardous seismic events.

In EGS, one clear trigger mechanism of seismicity is the fluid injection itself, which increases the pore pressure and reduces the normal effective stress along preexisting fractures and/or faults, therefore facilitating seismic slip. Based on that, most studies on induced seismicity only considered fluid flow and pore pressure changes as major cause of triggering for modeling and explaining injection-induced earthquakes [*Goertz-Allmann and Wiemer*, 2012; *Gischig and Wiemer*, 2013; *Hakimhashemi et al*., 2014; *Shapiro*, 2015, and references therein]. In these studies the possible effect of earthquake interactions driven by static stress redistribution was ignored. However, when an earthquake occurs the region nearby the nucleation point can

undergo instantaneous stress changes, and such changes, when positive, can be responsible of secondary activations at new locations. The static Coulomb stress change gives therefore an indication on subsequent shock locations. In the Basel case we can ignore dynamic stress transferring because no large earthquakes in the region were recorded before, during, and after active injection.

Catalli et al. [2013] have already shown that the static stress interactions by induced earthquakes might play a significant role in the triggering process in EGS experiments. *Schoenball et al*. [2012] concluded that the earthquake interaction is quite effective for rupture propagation along large fault zones. The seismicity in Basel has clear sign of reactivation along a somewhat large fault system, and the distribution of seismicity is oriented onto this major feature [*Deichmann et al*., 2014; *Kraft and Deichmann*, 2014]. *Baisch et al*. [2010] incorporated some simplified static stress transfer in numerical simulations. Such work shows also the importance of accounting static stress transfer. However, their formulation, so-called “block-spring model,” fails in describing zone of stress shadow, since the model only accounts for positive shear stress transfer at points near the reactivating patch.

Although it has become clearer that stress interactions can play a significant role as a triggering process also for injection-induced seismicity, a full understanding of the relation between the two different processes is yet not completely unraveled. Moreover, it remains to be unexplained whether implementing earthquake stress interactions might be important for induced seismicity forecasting models. Indeed, in such developments, physical complexity resulting in increased parameters space and computation time is only justified if hazard forecast is significantly improved.

The novelty of this study is analyzing the role of earthquake stress interactions for modeling injection-induced seismicity. Considering a model with both pressure transient evolution (i.e., pressure changes, ΔP, which reduce the effective normal stress) and static stress redistribution (referred to as Coulomb failure stress changes due to earthquake interactions, ΔCFS_{int}) as triggering mechanisms, we produce 1200 stochastic seismic catalogues to account for possible uncertainties.

We present an improved version of the “seed model” proposed by *Gischig and Wiemer* [2013] for simulating injection-induced seismicity by considering pressure transient evolution coupled with a stochastic seismicity model. We additionally consider earthquake interactions in terms of static stress redistribution as another possible triggering mechanism, as suggested by *Catalli et al*. [2013]. We treat the physical problem as a simplified, one-way coupled process, i.e., increased pressure induces earthquakes causing stress changes around the source, but slip associated with the earthquakes has no direct feedback on the permeability field. We further ignore the deformation caused by the injection itself (i.e., the poroelastic stress changes). We propose our approach as a simplified, although improved version of the

original seed model, which still leaves room for further developments to investigate on other significant and not yet included aspects.

The model parameters are calibrated against observations of the injection-induced seismic sequence of the EGS of Basel, Switzerland [*Häring et al*., 2008]. The stimulation of the EGS of Basel started on 2 December 2006 and lasted for 6 days, when a M_L 2.6 occurred and the injection was first reduced and then stopped. However, in the following 2 months other $M_L > 3.0$ occurred, among the thousand events induced and registered. A high level of seismicity is still visible just after the reduction and the end of injection, about 5–6 days after begin, as shown in Figure 5c by *Häring et al*. [2008]. For this sequence, *Catalli et al*. [2013] found that ΔCFS_{int} acts as an additional triggering mechanism, especially at later injection time.

Hence, we build on the model employing a nonlinear pressure transient evolution, a stochastic seismicity model, and static stress transfer able to reproduce the main characteristics of the induced seismicity observed during the injection in Basel [*Gischig and Wiemer*, 2013]. The goal of our work is to quantify the relative effect of including static earthquake interactions with respect to a simplified scenario with seismicity only induced by pore pressure changes.

2 Methodology

The methodology used in this study to simulate seismic catalogues for injection-induced events can be described by referring to three different modules, as shown in Figure 1: (1) a nonlinear 2-D pore pressure diffusion model (using the finite element modeling package COMSOL) [*Gischig and Wiemer*, 2013]; (2) a stochastic seismicity model, termed as seed model [*Goertz-Allmann and Wiemer*, 2012; *Gischig and Wiemer*, 2013]; and (3) the Coulomb failure stress model for static stress change estimations [*Catalli et al*., 2013, and references therein].

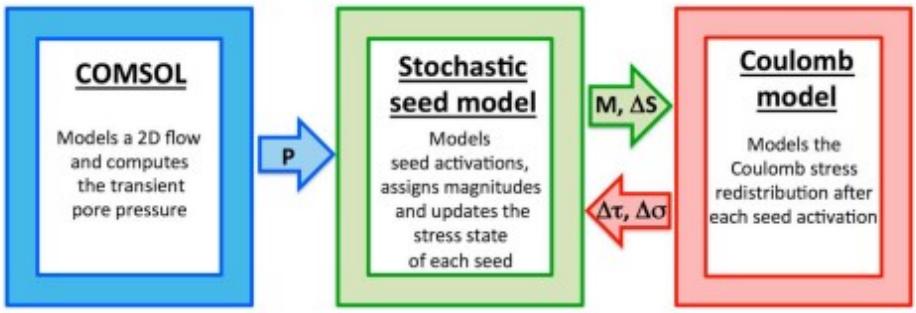

Figure 1. Scheme of the coupling among the three modules of the methodology: the fluid-flow, the seed, and the Coulomb failure stress models. *P* represents the transient pressure, *M* the magnitude, ΔS the stress drop, and $\Delta\tau$ and $\Delta\sigma$ the shear and normal stress changes.

Major assumptions of the 2-D fluid flow model can be summarized in the following points: the permeability, *k*, (1) increases irreversibly; i.e., it increases when pressure increases, but does not decrease when the

pressure drops; (2) increases only above minimum pressure threshold; (3) and increases only up to a limiting factor (maximum stimulation factor). The model assumes a homogenous initial permeability distribution in space. Pore pressure distribution evolves radially symmetric and does not account for preferential flow paths (see Figure 2a). A key point behind EGS is the increase in permeability following hydroshearing process [e.g., *Miller*, 2015; *Rinaldi et al*., 2015a]. Although we do not explicitly model the effects of fault reactivation on fluid flow, plastic effects are indirectly accounted for by assuming that the permeability enhancement is irreversible. Despite the simplifications, the fluid flow model is able to reproduce the reservoir pressure response, i.e., the wellhead pressure recorded in Basel. Further details about the fluid flow model can be found in *Gischig and Wiemer* [2013].

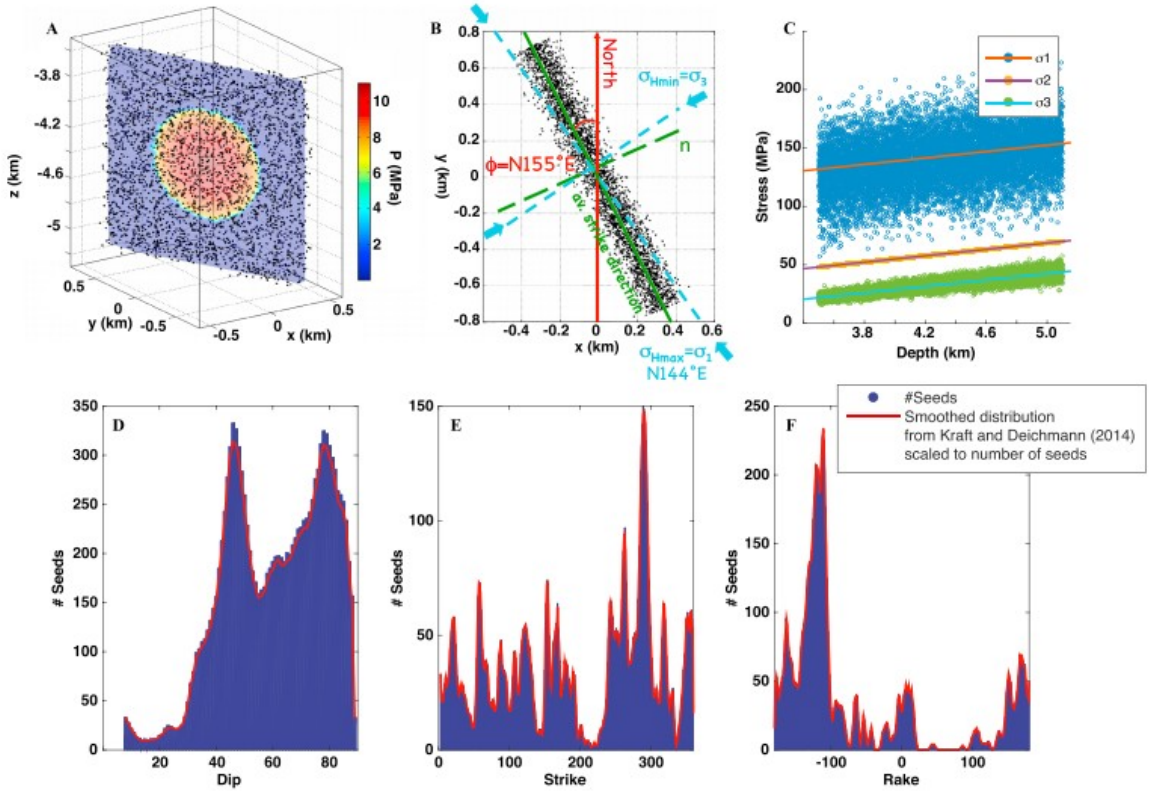

Figure 2. Sketch of the geometrical setup. (a) The pore pressure is modeled on a vertical plane of about 1000 m radius from the injection well; the depth of the open hole is fixed at 4.3 km. Initial seeds are randomly distributed all over this plane. (b) On the horizontal plane the cloud of seeds is rotated accordingly to the Basel event *M*l 3.5 strike, i.e., φ = N155°E [*Kraft and Deichmann*, 2014]. The orientation of the maximum principal stress σ_1 is of N144°E, as reported by *Valley and Evans* [2009]. (c) Stress assigned to the seeds as function of depth. (d–f) Distribution of dip, strike, and rake, respectively, as a smoothed distribution of catalogue by *Kraft and Deichmann* [2014].

The transient pressure evolution model is coupled to the seed model. Here we imagine a number of seed faults with different orientations uniformly random distributed over a subvertical plane at a depth of about 4.4 km, with a maximum radial distance from the casing shoe of 1000 m (Figure 2a). These seeds represent potential earthquake faults that can be activated by the transient ΔP. Seed fault activation occurs by means of the Mohr-Coulomb failure criterion based on the effective normal stress reduction, initially only

controlled by ΔP. The orientation of the cloud of seeds is assigned according to the Basel average distribution of seismicity (i.e., N155°E; Figure 2b), following the relocated catalogue by *Kraft and Deichmann* [2014]. We account for a full 3-D stress tensor: the principal stresses at each seed location are assigned with fixed orientation (i.e., N144°E [*Valley and Evans*, 2009]), and with normally distributed variability (10%) around an average, depth dependent value (Figure 2c). Each seed represents a fault zone, and each fault orientation (defined by dip, strike, and rake angles) was extrapolated from a scaled, smoothed distribution of observed fault plane solutions [*Deichmann et al*., 2014; *Kraft and Deichmann*, 2014]. Distribution of orientation scaled to the number of seeds is shown in Figures 2d–2f for dip, strike, and rake, respectively. Finally, shear and normal stresses at each seed location are calculated by means of a full stress tensor rotation [*Zoback*, 2010] and the failure pressure evaluated accordingly. For each seed, a *b*-value is calculated assuming a negative linear relationship with the differential stress at seed location [*Schorlemmer et al*., 2005; *Goertz-Allmann and Wiemer*, 2012; *Scholz*, 2015]. When a seed fault fails, the event magnitude is randomly drawn given the seed *b*-value defining at Gutenberg-Richter distribution. *Gischig and Wiemer* [2013] showed that this seed model along with the nonlinear pressure diffusion model is already able to realistically reproduce the time evolution and magnitude distribution of observed seismicity in Basel, as well as the total number of events. Indeed, several models [e.g., *Langenbruch et al*., 2011; *Bachmann et al*., 2012; *Kiraly et al*., 2014] are able to reproduce the Basel sequence (by calibrating model parameters). However, when interactions between earthquakes are neglected, a physical component of the entire process of injection-induced seismicity is missing.

In order to address such limitation, the activated seed faults become sources of local stress changes, ΔCFS_{int}, which in turn can trigger additional seeds. This constitutes the actual novelty of the model version used here: when a seed fault fails and becomes a source of ΔCFS_{int}, its stress perturbation might influence all the other seeds and favor new events to occur. For computing ΔCFS_{int}, the seed faults are given an off-plane coordinate to produce a more realistic 3-D seismicity cloud. For this reason, the x coordinates of the seeds are normally distributed in the off-plane-direction (i.e., normal to the 2-D fluid flow plane) with a cloud of seeds reaching a width of about 60 m. This assumption is also needed to allow for stress shadow at some seed locations; otherwise, the model would extremely over perform in terms of Coulomb stress changes, because all seeds would be aligned, hence in positive regions of ΔCFS [*King et al*., 1994]. The assumption of only 60 m width of the seismic cloud remains in agreement with the 2-D pore pressure model because of such a slight normal variation of x. Whether a seed fault is triggered (or re-triggered) or not is again decided by estimating the effective stress reduction, this time controlled by a superposition of the contributions coming from both ΔP and ΔCFS_{int} and using always the Mohr-Coulomb

criterion. For ΔCFS_{int} estimations, dimension of sources, and magnitude of slip are calculated from the stress drop and seismic moment magnitude by following empirical relationships [e.g., *Hanks and Kanamori*, 1979; *Wells and Coppersmith*, 1994]. Therefore, for the application of the Coulomb model the seed faults are treated as rectangular sources, as required by the stress calculation formulated by *Okada* [1992]. Stress redistribution alters the stress state of each receiver seed, and this is considered for each time step in the spanned time-window. Stress drop is calculated as a percentage of the stress condition at reactivating seed [*Goertz-Allmann et al.*, 2011]. Such drop is applied to a region nearby the triggered seed points, therefore enabling also re-triggering caused by a further stress variation if conditions are satisfied.

We refer the reader to previous mentioned studies for more specific details on the fluid flow and stochastic seismicity modules here just shortly described.

The model parameters, listed in Table 1, were calibrated to achieve a reasonable matching with the EGS of Basel. For the fluid flow model detailed calibration on Basel and description of the hydraulic parameters involved refer to *Gischig and Wiemer* [2013].

Table 1. Major Parameters Used for the Model Setup[a]

Fluid Flow Model [*Gischig and Wiemer*, 2013]	
Open-hole section	371 m
Initial permeability	6.61e-18 m^2
Transmissivity	2.45e-15 m^3
Storage	5.14e-12 Pa^{-1}
Water viscosity	2.5e-4 Pa s
Water density	970 kg m^{-3}
Seed model (modified after *Gischig and Wiemer* [2013])	
Seed density, N	13,000 seeds per $1.0 \times 1.0 \times 0.06$ km^3
Cohesion, C	2.0 MPa
Criticality, μ_c	0.01
Stress drop parameter, $\mu_{\Delta\tau}$	0.05
Frictional coefficient, μ	0.65 ± 0.15
Coulomb model	
Friction coefficient, μ	0.65
Strike, dip and rake (sources and receivers)	Smoothed distribution following *Kraft and Deichmann* [2014]
Elastic parameters, λ, μ	30 GPa
Skempton coefficient, B	0.5
Source rigidity at depth	30 GPa

[a]The criticality coefficient μ_c introduces a gap between the seeds closest to failure and the failure envelope itself; the stress-drop parameter $\mu_{\Delta\tau}$ represents the proportionality between the normal stress and the stress drop after failure. They are both free parameters used in the seed model for calibration.

3 Discussion of Results

The results shown in this section represent the average behavior of each studied quantity estimated over 1200 realizations together with its standard deviation.

The first significant result that we obtain is the relatively increased number of triggered seeds, as shown in Figures 3a and 3c. Considering the same set of parameters (Table 1), the rate of triggered events when considering earthquake interactions (Figure 3a) is especially higher (compared to the case of no interactions, shown in Figure 3b) around the time of the injection reduction and the shut-in of the well (approximately 5 and 6 days after injection began). This rate behavior, observed when also interactions are considered as a triggering mechanism, reproduces the observations reported in Figure 5c of *Häring et al*. [2008]. Consequently to the increased rate of triggered seeds at some times, also the total number of triggered seeds increases when considering ΔCFS_{int} (Figure 3c) and can reproduce the time behavior of the total number of observations in Basel by using the parameters listed in Table 1. It is worth noting that a formulation with seismicity only induced by pressure changes could also reproduce the observed total number and rate of events [*Gischig and Wiemer*, 2013], by changing for example parameters such as cohesion, frictional coefficient, and/or number of seeds. However, for a given set of parameters, the inclusion of earthquake interactions will cause a larger number of events. Such increase is more pronounced toward the end of the stimulation phase and after shut-in, with a 24% larger total number of events when compared to a case with only pressure as triggering mechanism.

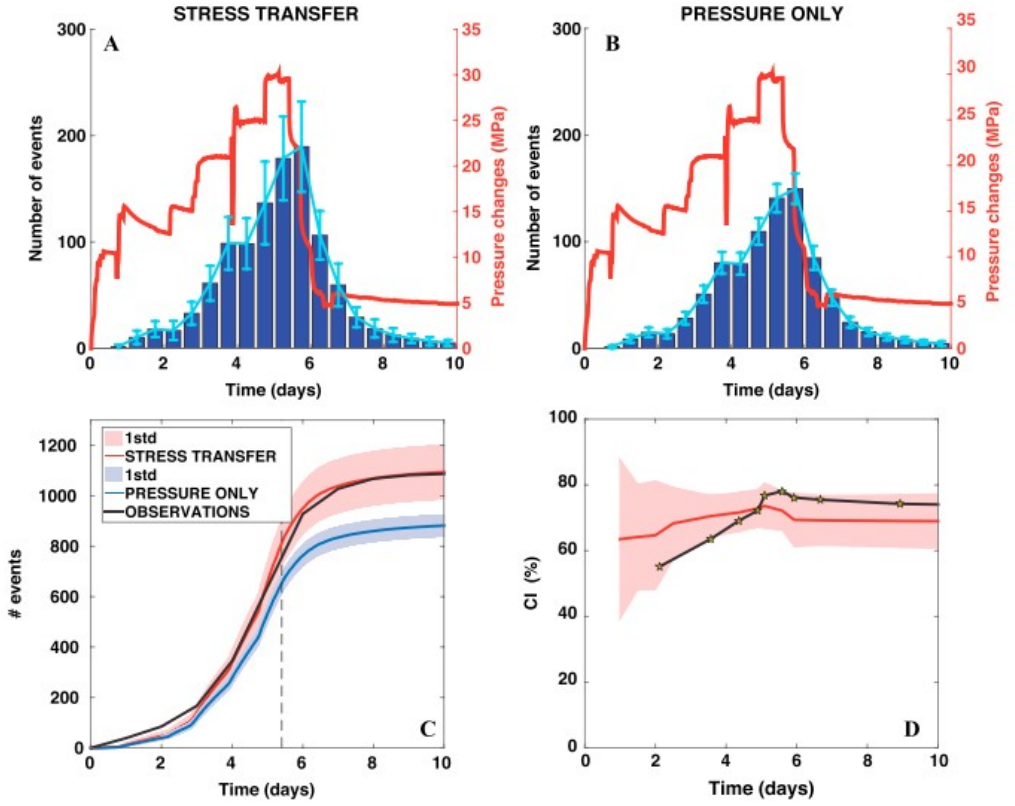

Figure 3. Time behavior of the daily rate, the total number of expected events, and the Coulomb index (CI). (a and b) The daily rate of events expected when considering: both pore pressure and interactions as triggering mechanisms (Figure 3a) and only the pressure (Figure 3b). The red line represents the simulated transient pore pressure at wellhead. (c and d) The total number of events (with or without interactions considered, in comparison with observations) and the time trend of the CI (for model in red and real data in black). Panels show average values estimated over 1200 realizations and their standard deviations.

We also tried to reproduce the time trend of the Coulomb Index, CI (i.e., the percentage of events that occur in locations with positive cumulative ΔCFS_{int} [*Hardebeck et al*., 1998]). We calculated the CI for Basel following the work by *Catalli et al*. [2013] and taking into consideration the cluster analysis by *Deichmann et al*. [2014]. Recently, *Kraft and Deichmann* [2014] performed a comprehensive analysis of the seismicity recorded at six borehole stations. Their results feature a fault plane solution for over 600 events and provide some essential information on the possible reactivation mechanisms. We accounted for such information on the distribution of our seeds throughout the domain as explained above. However, the focal mechanisms derived by *Kraft and Deichmann* [2014] are less constrained than the ones obtained by *Deichmann et al*. [2014], whose analysis relies on a catalogue recorded at the surface seismic network. Therefore, for the calculation of the CI of the Basel sequence, we prefer to account only for a subset of events (~170). If a given event was not assigned to a cluster by *Deichmann et al*. [2014], we accounted for the regional stress orientation to discriminate between preferential and auxiliary fault plane solution.

In Figure 3d we show the temporal trend of modeled CI (red line) in comparison with the observed one (black line). Overall, the model is able to capture the main trend variation within the statistical variation over 1200 realizations. Differences, particularly at early time, are attributed to the simplification of working with a 2-D pressure model. Figure 3d captures the limit of our modeling: to stay in agreement with the 2-D fluid-flow model (i.e., not considering diffusion on the third dimension) it is reasonable to assume a relative small width of the cloud; on the other hand, it would be more realistic to assume that initial potential faults were distributed in a volume and just after the process starts event could develop along preferential paths (e.g., with enhanced permeability), as observed in Basel. This would correspond to a two-way coupled fluid flow model [e.g., *Gischig et al*., 2014; *Rinaldi et al*., 2015a; *Nespoli et al*., 2015], which might represent the underlying physics of reservoir stimulation more appropriately. We further note that the simulated and observed time behaviors of CI are based on a large difference of contributing events for ΔCFS_{int} in the case of observations in Basel and in case of the model (about 170 for the real Basel case, for which focal mechanisms were known and reliable, and about 1100 for the simulations). Nevertheless, the methodology catches the overall increase of the CI in time, which is the most significant characteristic of the observed CI trend. This is related to the increased weight of the mutual earthquake interactions in time as triggering mechanism with respect to the transient pore pressure variation. This result confirms the hypothesis already proposed by *Catalli et al*. [2013] that two different phases are recognizable during an induced seismic sequence: (1) at early times during injection and closer to the injection well, the seismicity triggering is controlled by the significant pore pressure perturbation; (2) at later times the process becomes more sensitive to earthquake interactions because stress changes accumulate while ΔP starts decreasing. This feature of induced seismicity is reproduced by our methodology and shown in Figure 4, where we trace the percentage of the two trigger contributions with time and distance from the injection, for the case where the earthquake interactions are included. Figure 4a confirms that while the importance of triggering by ΔP decreases with time, on the other hand the one by ΔCFS_{int} increases. Results show that at the end of the stimulation about 26% of the events are primarily triggered by earthquake interaction. Note that we cannot distinguish between the independent contributions of the two triggering mechanisms because they contribute together and indissolubly to the triggering process by accumulating stress change; however, we can determine at each time step and for each failing seed the determining trigger; i.e., if the failure is eventually reached due to a stress variation by ΔP or ΔCFS_{int}. Figure 4b shows the same concept of the determining trigger against the distance of failing seeds from the injection point. Figure 4b shows that while at relative close distances to the injection (within about 200 m) the two phenomena act in synergy, farther away ΔP predominates (its diffusion probably playing a main role). However, outside the pressurized zone, and even farther away from injection (i.e., distance

greater than 650 m), the ΔCFS_{int} is the only mechanisms triggering seismicity, in accordance what the findings by *Catalli et al*. [2013]. The results in Figure 4b show then that the interactions among earthquakes are more effective within the stimulated volume as absolute value, but if seismicity is occurring outside the pressurized zone, it can only caused by ΔCFS_{int}. This is well in agreement with a stimulated reservoir that is more critically stressed with respect to the host rock, hence more prone to have interactions among faults. Moreover, the results of simulation well agree with the intuitive concept that if an event occurs in a region presumably not pressurized, the trigger mechanisms can only be due to stress variation. *Bachmann et al*. [2011] showed that the *b*-value is high within the stimulated reservoir only to decrease to a tectonic value farther away from injection. This feature can be interpreted as a signature of the solely earthquake interaction in space, where the pressure effect is negligible (Figure 4b)

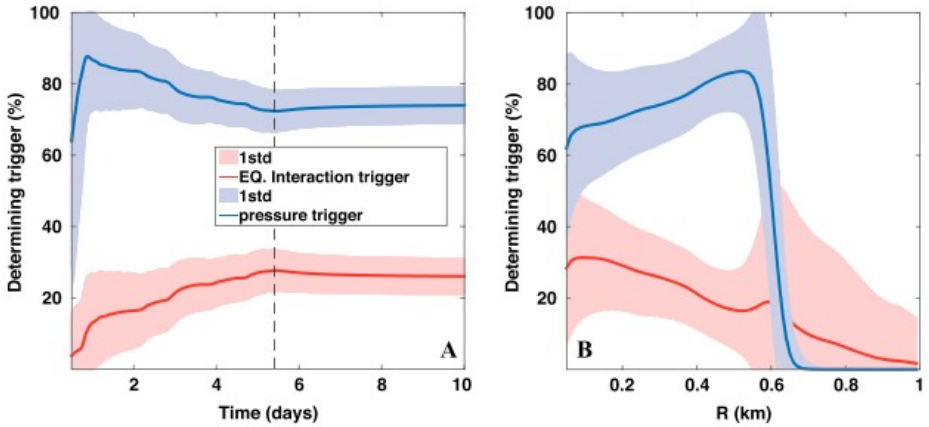

Figure 4. (a) Time and (b) spatial trend of the determining trigger in percentage, i.e., the rate of failing seeds triggered by an accumulation of stress where the last and decisive change is a ΔP (blue line) or a ΔCFS_{int} (red line). *R* represents the distance between the seed and the injection point. The results represent the average trend over 1200 realizations.

4 Conclusions

The goal of this study is to quantify the influence of static stress changes due to earthquake mutual interactions during an injection-induced seismic sequence.

This paper agrees with the findings of *Catalli et al*. [2013] about the significant role of Coulomb stress redistribution due to earthquake interactions during a fluid-induced seismic sequence; however, the analysis proposed here is more general and based on a statistical approach; indeed, we forward model synthetic earthquake catalogues, taking into account stochastic variability and uncertainties of variables.

The methodology presented in this study is an improved version of the seed model already proposed by *Goertz-Allmann and Wiemer* [2012] and *Gischig and Wiemer* [2013]; the novelty of the new approach is the implementation of the Coulomb failure model for reproducing static stress redistribution after

event interactions. Although the model is yet based on simplistic assumptions compared with the complexity of the real problem, we can reproduce the overall behavior of observed seismicity significantly well. Furthermore, it also reproduces the relative importance of Coulomb stress interaction observed by *Catalli et al*. [2013].

The major results of this study can be summarized in the following points: (1) By considering the stress changes from event interactions as an additional triggering mechanism of induced seismicity, the methodology shows how that number of events is significantly increased (24% more) compared to a case of seismicity triggered by pressure changes only. (2) We verify the existence of two different phases of triggering in an injection-induced sequence type, where the determining trigger factors are ΔP and ΔCFS_{int}, respectively. (3) The earthquake interactions are generally more effective within the stimulated reservoir, but if events occur outside the pressurized region, these are only triggered by ΔCFS_{int}.

The model is based on assumptions that can be improved by reconsidering the level of complexity of the whole methodology, for example, by introducing the poroelastic response [*Segall and Lu*, 2015], or transient permeability changes [e.g., *Gischig et al*., 2014]. Although the focus of this work is the earthquake interaction for injection-induced seismicity, we currently recognized as major limitation of the model the 2-D assumption. The Coulomb model for earthquake interactions is particularly sensitive to the relative locations of faults in the volume, and for this reason we believe that a significant improvement of the methodology is represented by the implementation of a 3-D fluid-flow model, even though recent modeling efforts have shown how a proper 2-D scaling does not affect the geomechanics of the system [*Rinaldi et al*., 2014, 2015b].

Finally, while the earthquake interactions may play a role in the physical understanding of the processes underlying EGS stimulation, the inclusion of such phenomenon in real-time forecasting is difficult to achieve and computationally expensive. On the other side, changing some modeling parameters in a pressure-only model (e.g., coefficient of friction and cohesion) may as well lead to an increase in number of events, similar to the effect caused by including the earthquake interactions.

Acknowledgments

We are grateful to GeoPower Basel for permission to use data regarding the Basel injection test and seismic sequence. Data associated with this study can be obtained upon request by contacting the corresponding author at flaminia.catalli@gfz-potsdam.de. The authors are grateful to Sebastian Hainzl, Men-Andrin Meier, and Toni Kraft for their valuable comments and inspiring discussions. A.P. Rinaldi is currently funded by Swiss National Science Foundation Ambizione Energy grant (PZENP2_160555). Comments from two anonymous reviewers greatly helped improving the early version of the manuscript.

References

Bachmann, C. E., S. Wiemer, J. Woessner, and S. Hainzl (2011), Statistical analysis of the induced Basel 2006 earthquake sequence: Introducing a probability-based monitoring approach for Enhanced Geothermal System, *Geophys. J. Int.*, 186, 793– 807, doi:10.1111/j.1365-246X.2011.05068.x.

Bachmann, C. E., S. Wiemer, B. P. Goertz-Allman, and J. Woessner (2012), Influence of pore-pressure on the event-size distribution of induced earthquakes, *Geophys. Res. Lett.*, 39, L09302, doi:10.1029/2012GL051480.

Baisch, S., R. Vörös, E. Rothert, H. Stang, R. Jung, and R. Schellschmidt (2010), A numerical model for fluid injection induced seismicity at Soultz-sous-Forêts, *Int. J. Rock Mech. Min. Sci.*, 47, 405– 413, doi:10.1016/j.ijrmms.2009.10.001.

Catalli, F., M.-A. Meier, and S. Wiemer (2013), The role of Coulomb stress changes for injection-induced seismicity: The Basel enhanced geothermal system, *Geophys. Res. Lett.*, 40, 72– 77, doi:10.1029/2012GL054147.

Deichmann, N., T. Kraft, and K. Evans (2014), Identification of faults activated during the stimulation of the Basel geothermal project from cluster analysis and focal mechanisms of the larger magnitude events, *Geothermics*, 52, 84– 97, doi:10.1016/j.geothermics.2014.04.001.

Evans, K. F., A. Zappone, T. Kraft, N. Deichmann, and F. Moia (2012), A survey of the induced seismic responses to fluid injection in geothermal and CO_2 reservoirs in Europe, *Geothermics*, 41, 30– 54, doi:10.1016/j.geothermics.2011.08.002.

Gischig, V., and S. Wiemer (2013), A stochastic model for induced seismicity based on non-linear pressure diffusion and irreversible permeability enhancement, *Geophys. J. Int.*, 194, 1229– 1249, doi:10.1093/gji/ggt164.

Gischig, V., S. Wiemer, and A. Alcolea (2014), Balancing reservoir creation and seismic hazard in enhanced geothermal systems, *Geophys. J. Int.*, 198, 1585– 1598, doi:10.1093/gji/ggu221.

Goertz-Allmann, B. P., and S. Wiemer (2012), Geomechanical modeling of induced seismicity source parameters and implications for seismic hazard assessment, *Geophysics*, 78, 25– 39, doi:10.1190/geo2012-0102.1.

Goertz-Allmann, B. P., A. Goertz, and S. Wiemer (2011), Stress drop variations of induced earthquakes at the Basel geothermal site, *Geophys. Res. Lett.*, 38, L09308, doi:10.1029/2011GL047498.

Hakimhashemi, A. H., M. Schoenball, O. Heidbach, A. Zang, and G. Grünthal (2014), Forward modelling of seismicity rate changes in georeservoirs with a hybrid geomechanical-statistical prototype model, *Geothermics*, 52, 185– 194, doi:10.1016/j.geothermics.2014.01.001.

Hanks, T. C., and H. Kanamori (1979), A moment-magnitude scale, *J. Geophys. Res.*, 84, 2348– 2350, doi:10.1029/JB084iB05p02348.

Hardebeck, J., J. Nazareth, and E. Hauksson (1998), The static stress change triggering model: Constraints from two southern California aftershock sequences, *J. Geophys. Res.*, 103(B10), 24,427– 24,437, doi:10.1029/98JB00573.

Häring, M., U. Schanz, F. Ladner, and B. Dyer (2008), Characterisation of the Basel enhanced geothermal system, *Geothermics*, 37, 469– 495, doi:10.1016/j.geothermics.2008.06.002.

King, G. C. P., R. S. Stein, and J. Lin (1994), Static stress changes and the triggering of earthquakes, *Bull. Seismol. Soc. Am.*, 84, 935– 953.

Kiraly, E., V. Gischig, D. Karvounis, and S. Wiemer (2014), Validating models to forecasting induced seismicity related to deep geothermal energy projects, in *Proceedings of 39th Workshop on Geothermal Reservoir Engineering*, Stanford Univ., Stanford, Calif., 24-26 Feb., SGP-TR-202.

Kraft, T., and N. Deichmann (2014), High-precision relocation and focal mechanism of the injection-induced seismicity at the Basel EGS, *Geothermics*, 52, 59– 73, doi:10.1016/j.geothermics.2014.05.014.

Langenbruch, C., C. Dinske, and S. A. Shapiro (2011), Inter events times of fluid induced earthquakes suggest their Poisson nature, *Geophys. Res. Lett.*, 38, L21302, doi:10.1029/2011GL049474.

Miller, S. A. (2015), Modeling enhanced geothermal systems and the essential nature of large-scale changes in permeability at the onset of slip, *Geofluids*, 15(1–2), 338– 349, doi:10.1111/gfl.12108.

Nespoli, M., A. P. Rinaldi, and S. Wiemer (2015), TOUGH2-SEED: A coupled fluid flow mechanical-statistical model for the study of injection-induced seismicity, in *Proceeding of the TOUGH Symposium 2015*, *Lawrence Berkeley National Laboratory*, Berkeley, Calif., 28-30 Sept.

Okada, Y. (1992), Internal deformation due to shear and tensile faults in a half-space, *Bull. Seismol. Soc. Am.*, 82, 1018– 1040.

Rinaldi, A. P., V. Vilarrasa, J. Rutqvist, and F. Cappa (2014), 3D modeling of fault reactivation during CO_2 injection, Abstract H11K-05 presented at 2014, Fall Meeting, AGU, San Francisco, Calif., 15-19 Dec.

Rinaldi, A. P., J. Rutqvist, E. L. Sonnenthal, and T. T. Cladouhos (2015a), Coupled THM modeling of hydroshearing stimulation in tight fractured volcanic rock, *Transp. Porous Media*, 108, 131– 150, doi:10.1007/s11242-014-0296-5.

Rinaldi, A. P., V. Vilarrasa, J. Rutqvist, and F. Cappa (2015b), Fault reactivation during CO_2 sequestration: Effects of well orientation on seismicity and leakage, *Greenhouse Gases Sci. Technol.*, 5, 645– 656, doi:10.1002/ghg.1511.

Schoenball, M., C. Baujard, T. Kohl, and L. Dorbath (2012), The role of triggering by static stress transfer during geothermal reservoir stimulation, *J. Geophys. Res.*, 117, B09307, doi:10.1029/2012JB009304.

Scholz, C. H. (2015), On the stress dependence of the earthquake *b* value, *Geophys. Res. Lett.*, 42, 1399– 1402, doi:10.1002/2014GL062863.

Schorlemmer, D., S. Wiemer, and M. Wyss (2005), Variations in earthquake-size distribution across different stress regimes, *Nature*, 437, 539– 542, doi:10.1038/nature04094.

Segall, P., and S. Lu (2015), Injection-induced seismicity: Poroelastic and earthquake nucleation effects, *J. Geophys. Res. Solid Earth*, 120, 5082– 5103, doi:10.1002/2015JB012060.

Shapiro, A. S. (2015), *Fluid-Induced Seismicity*, pp. 283, Cambridge Univ. Press, New York.

Valley, B., and K. Evans (2009), Stress orientation to 5 km depth in the basement below Basel (Switzerland) from borehole failure analysis, *Swiss J. Geosci.*, 102, 467– 480, doi:10.1007/s00015-009-1335-z.

Wells, D. L., and K. J. Coppersmith (1994), New empirical relationship among magnitude, rupture length, rupture width, rupture area, and surface displacement, *Bull. Seismol. Soc. Am.*, 84, 974– 1002.

Zang, A., V. Oye, P. Jousset, N. Deichmann, R. Gritto, A. McGarr, E. Majer, and D. Bruhn (2014), Analysis of induced seismicity in geothermal reservoirs – An overview, *Geothermics*, 52, 6– 21, doi:10.1016/j.geothermics.2014.06.

Zoback, M. D. (2010), *Reservoir Geomechanics*, pp. 449, Cambridge Univ. Press, New York.